DANISH METEOROLOGICAL INSTITUTE

SCIENTIFIC REPORT

98-13

Microphysical analysis of polar stratospheric clouds observed by lidar at McMurdo, Antarctica

By

N. Larsen,
Alberto Adriani
Guido Di Donfrancesco

DMI

COPENHAGEN 1998

Danish Meteorological Institute, Division of Middle Atmosphere Research,
Lyngbyvej 100, DK-2100 Copenhagen Ø, Denmark

ISBN 87-7478-380-7
ISSN 0905-3263

Microphysical analysis of polar stratospheric clouds observed by lidar at McMurdo, Antarctica

Niels Larsen
Danish Meteorological Institute

Alberto Adriani and Guido Di Donfrancesco
Instituto per la Fisica dell' Atmosfera
Consiglio Nazionale Delle Ricerche

Introduction.

As part of the CEC funded research project "Multi-Instrument Investigation of Polar Stratospheric Cloud Formation and Heterogeneous Chemistry Involved in Stratospheric Ozone Depletion" (POSTCODE, contract ENV4-CT97-0541) Dr. Niels Larsen, DMI, has been working at CNR-IFA in the period 23 June – 17 July, 1998. The objective of the visit has been to initiate analysis of Antarctic lidar observations of Polar Stratospheric Clouds (PSC) by means of microphysical model simulations, based on temperature histories from isentropic air parcel trajectory calculations.

Background.

Polar stratospheric clouds play a mandatory role for stratospheric chemical ozone depletion in early spring. Heterogeneous chemical reactions on the surfaces of the cloud particles convert inactive chlorine compounds into potential ozone destroying radicals. Secondly, by the particle uptake of HNO_3 and H_2O and gravitational sedimentation of the largest cloud particles, reactive nitrogen and water is irreversibly removed from the altitudes where the clouds form (denitrification and dehydration). Denitrification prolongs the lifetime of halogen radicals and thereby increases the ozone depletion. The heterogeneous chemical reaction rates depend on the particle surface area, particle composition and physical phase, and an efficient denitrification depends specifically on processes leading to the formation of a small number of relatively large solid PSC particles. In order to perform a more accurate modelling of stratospheric ozone depletion, details of the microphysical processes involved in PSC formation must be known. However, many uncertainties remain, in particular regarding the phase transformations between liquid and solid PSC particles and the formation of large solid particles.

The initial stages of PSC formation are of particular interest since this provide the opportunities to study the important processes of phase changes. In the Arctic winter temperatures hover around the thresholds for PSC formation and thereby PSC are often observed in the initial states of formation throughout the winter. In contrast, Antarctic winter stratosphere temperatures are lower and the evolution in PSC formation from the initial stages, characterised by mixtures of liquid, solid and

perhaps metastable solid phases, into more mature and aged PSCs, characterised by solid particles, can be studied.

Lidar measurements.

The CNR-IFA possesses a comprehensive database of PSC lidar observations from the Antarctic McMurdo station from all winters since 1991. Lidar measurements (wavelength 532 nm) are particularly suited to study phase changes among atmospheric particles since solid particles, in contrast to liquids, give rise to depolarisation of the backscattered laser signal and thereby information of the physical state of the particles. The aim of the work has been to identify cases among the observations of PSC occurrences in the early winter season with clear signatures of mixtures of liquid and solid particles.

Cases from the winter 1996 and 1997 have been identified in the lidar database, which show mixtures of liquid and solid particles. The dates of observation of these first studied cases appear in the table together with the altitudes where backward isentropic air parcel trajectories have been provided from the NASA GSFC automailer trajectory model.

Case #	Date, time (UT)	Altitude (km)	Pot. Temperature (K)
1	960702-23.00	14.5	378
2	-	17.3	415
3	-	20.0	470
4	-	22.0	525
5	960703-06.30	14.5	370
6	-	23.0	570
7	960704-01.00	12.2	350
8	-	17.0	410
9	-	23.0	570
10	960705-01.30	14.0	370
11	-	17.0	410
12	-	24.0	530
13	960724-01.30	16.3	400
14	-	25.0	650
15	970620-02.05	17.6	420
16	-	20.0	470
18	-	22.5	535
19	970622-07.40	17.0	408
20	-	22.0	515
21	970624-00.40	18.0	430
22	-	21.5	505
23	-	23.6	575
24	970629-00.05	16.0	402
25	-	17.5	422
26	-	21.0	495

The vertical profiles of total backscatter ratio and contributions to this from liquid and solid particles appear in Figure 1. All cases have been analysed by the 2nd version of the DMI microphysical PSC simulation model, using the provided temperature histories.

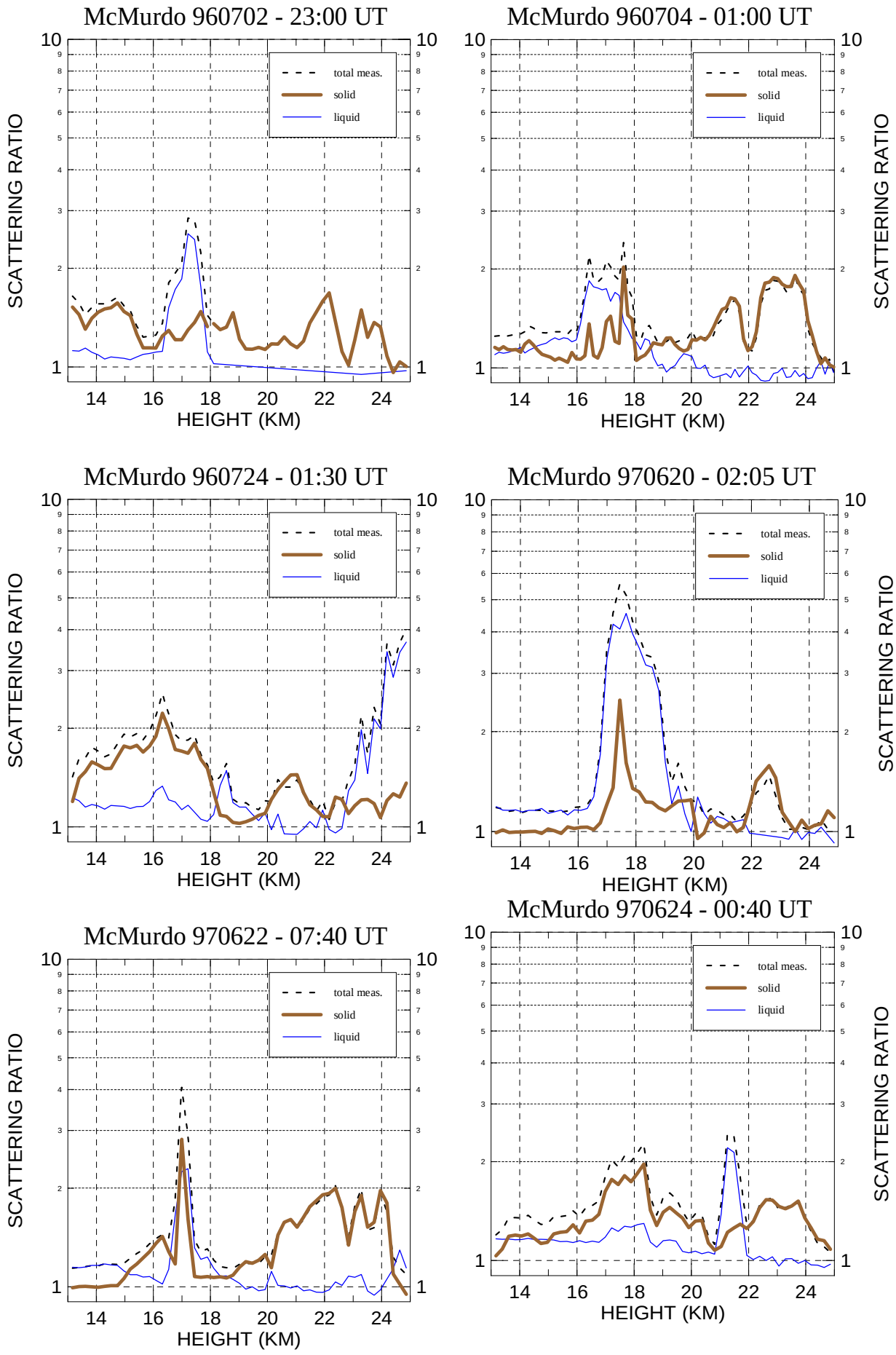

Figure 1. Vertical profiles of total backscatter ratio (dashed) and contributions to this from solid (thick line) and liquid particles (thin line). The observations have been used in the microphysical analysis.

Microphysical PSC model.

The microphysical model (Larsen, 1991) calculates the temporal evolution of particle size distributions and chemical composition in an ensemble of liquid and frozen stratospheric aerosols and polar stratospheric clouds. Basically, two types of stratospheric particles are modelled by this model: liquid and solid particles. The liquid particles are stratospheric sulfate aerosol particles which, at low temperatures, take up HNO_3 and H_2O by condensation, changing the composition into supercooled ternary solutions (STS; $HNO_3/H_2SO_4/H_2O$), also referred to as type 1b PSCs. The model allows for simulation of non-equilibrium uptake of HNO_3 in fast cooling/heating events (e.g. mountain lee-waves), employing a radius dependent chemical composition of the particles. The solid particles are grouped into three categories, depending on the chemical composition. The available water in each solid particle is assumed to be bound by 4 H_2O molecules to each one H_2SO_4 molecule, forming sulfuric acid tetrahydrate (SAT), and by 3 H_2O molecules to each one HNO_3 molecule, forming nitric acid trihydtate (NAT). Any H_2O molecules left not bound in hydrates, are assumed to form water ice (excess ice). Particles with excess ice are classified as type 2 PSCs. Particles with no excess ice but holdning HNO_3 (NAT) are classified as type 1a PSCs. Particles with no excess water and no HNO_3 (NAT) are classified as solid stratospheric aerosols (SAT particles).

The model takes as input the ambient air state variables: temperature, pressure, partial pressure of water vapor, and partial pressure of nitric acid vapor. The partial pressures are changed according to the evaporation/condensation taking place. The model calculates the time dependent radius and physical phase of each particle type, holding the number of particles per kg. air in each radius class fixed (Lagrangian approach in radius space). The mass of condensed H_2SO_4, HNO_3, and H_2O per particle (chemical composition) is calculated in each radius class due to condensation/evaporation, assuming a constant H_2SO_4 content.

Currently, the freezing mechanism of ternary solutions is unknown. In the model homogeneous volume dependent freezing of HNO_3/H_2O supercooled solutions is assumed (Tabazadeh et al.; 1997; Larsen et al., 1997; Larsen and Knudsen, 1998). Any frozen particles are assumed to melt when the air temperature is above the SAT melting temperature. SAT particles are assumed to dissolve upon cooling when the condition reach an HNO_3/NAT saturation ration larger than 15, followed by HNO_3 condensation to form NAT and type 1a PSC particles (cf. Iraci et al., 1998).

An optical model is used to calculate the particle volume backscatter coefficient (at 532 nm) and extinction coefficient (at 1 micron) of spherical particles, characterized by a differential size distribution, as calculated by the microphysical model (Larsen, 1992). The particles are assumed to be characterised by the refractive index (real part) of STS (Luo et al., 1996; U. Krieger, personal communication, 1998).

A number of problems have been identified when applying microphysical model analysis of the lidar observations, based on isentropic backward temperature histories. In several cases the temperature histories do not hold information on the possible freezing processes which have taken place prior to the lidar observations. This is mainly when temperatures have stayed in the range between the NAT condensation temperature and the ice frost point throughout the 7 days of backward trajectory calculations. In other cases the trajectory temperatures appear to be too high for PSC particles to exist although observed by the lidar. Another problem in this type of analysis is the assumed gas phase concentrations of water and nitric acid. The homogeneous freezing rate depends strongly on the H_2O partial pressure (Larsen and Knudsen, 1998), and the growth of STS particles (type 1b PSCs) is also strongly dependent on the amount of HNO_3 in the gas phase. In the simulations carried out in this initial study, Antarctic UARS nitric acid vapor profiles from 1995/1996 have been applied. Several observations show a “sandwich” vertical structure with a 1-2

km thick layer of dominantly liquid particles, appearing typically around 17-18 km altitude and surrounded above and below by solid particles. The liquid particle layers often appear to originate as intrusions of air from outside the Antarctic polar vortex, possibly carrying more water vapor than observed inside the vortex edge, making the analysis more difficult. A number of the cases which initially have studied will be described in the following.

Case studies.

On 2 July 1996 the lidar profile shows a liquid/solid mixture of predominantly solid particles at 14.5 km (378 K pot. temp.; case 1) and liquids at 17.3 km (415 K pot. temp.; case 2), cf. Fig 1, upper left panel. The results of the microphysical simulations are shown in Fig. 2 and 3 and will be used, first to give a description of the model output and also to discuss some of the difficulties in the analysis, using backward trajectories.

In the following all figures are of the same type, showing various model-calculated variables in 6 panels. The **upper left panel** shows the temperature (black), NAT condensation temperature (green), and ice frost point temperature (blue). The condensation temperatures are calculated corresponding to the actual gas phase concentrations. When condensation takes place and removes HNO_3 and H_2O from the gas phase, T_{NAT} and T_{ice} decrease and become equal to the air temperature when NAT, respectively ice particles, are in equilibrium with the gas phase. The **middle left panel** shows the saturation ratios over NAT (green) and ice (blue), and the **lower left panel** shows the gas phase mixing ratios of HNO_3 (green) and H_2O (blue). The **upper right panel** shows the radius of particles in each size class, red curves for liquid and blue curves for solid particles. The **middle right panel** shows the volumes of different types of particles: red: STS type 1b PSC (sulfate aerosols); green: solid type 1a PSC; blue: solid type 2 PSC, yellow: solid SAT particles, and black: total volume. The **lower right panel** shows the nitric acid weight fractions in the different size classes (black), the volume averaged nitric acid weight fraction (blue), and volume averaged sulfuric acid weight fraction in all particles.

The temperature histories leading to freezing of particles around day 179-180 are nearly the same in cases 1 and 2 with no melting after freezing (Fig. 2 and 3). The freezing mechanism must be size selective since the lidar observations show mixtures of liquids and solids; mostly solid particles at 378 K potential temperature (14.4 km) and mostly liquid particles at 415 K (17.3 km). The simulations show the same features with ice particle formation out of a relatively large fraction of the liquids at 378 K and only formation of a small number of solids at 410 K. This leaves behind a large fraction of liquid STS particles at the time of observation, where the particles take up most of the nitric acid from the gas phase, growing to liquid volumes more than 1 micron^3/cm^3. The backscatter ratio of these liquid particles is calculated to 2.2 in good agreement with the observations. The results are strongly dependent on the assumed H_2O mixing ratio. If the assumed H_2O mixing ratio is lowered from 7 to 6 ppmv at the 378 K level no freezing takes place. Also at the 415 K level are the results strongly dependent on the assumed H_2O concentrations. The reason that only a small fraction of the liquids freeze is due to the temperatures decreasing only slightly below the threshold for freezing. If the H_2O concentrations were raised to 6 ppmv all particles would freeze, leaving behind a fully developed type 2 cloud at the end which, on the other hand, is not in agreement with the observations. Finally, it should be mentioned that the few solid particles observed at the 410 K level could be explained by infall from layers above.

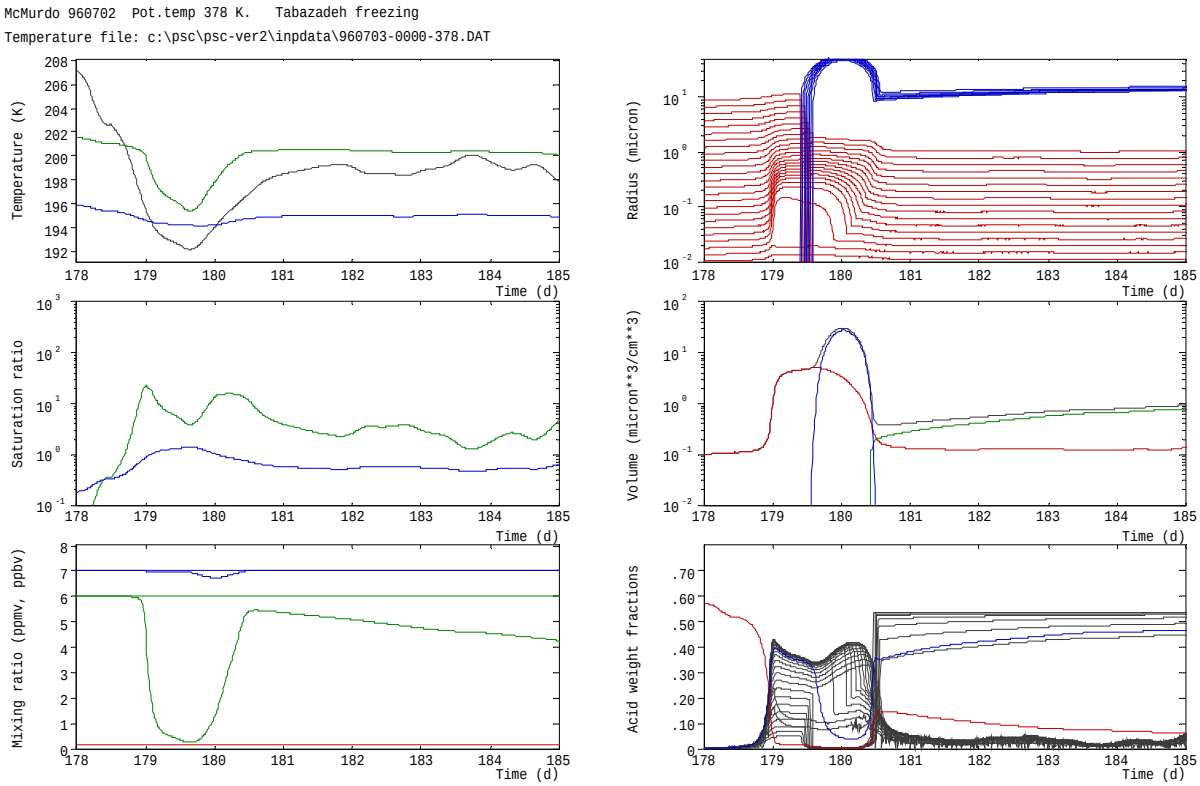

Figure 2

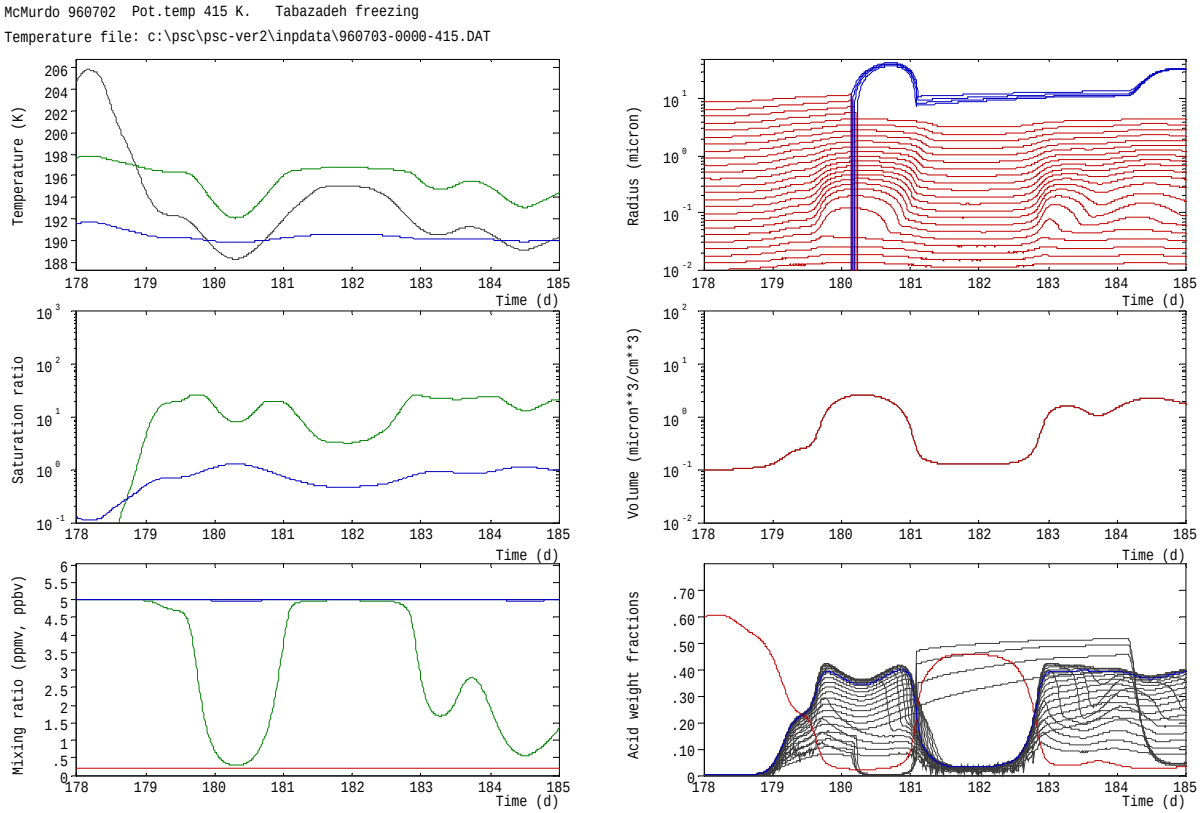

Figure 3

Fig. 4 shows that the simulations are strongly dependent on the accuracy of the temperatures. In these simulations the 378 K level temperatures have been overlaid by a sinusoidal temperature oscillation with a period of 0.5 day and an amplitude of 1 K. In this case the solid particles develop a broader size distribution with a larger number of smaller type 1a PSC particles. These particles are able to take up HNO_3 by condensation much faster than the relative large particles in the Fig. 2 simulation, and a fully developed NAT cloud appear.

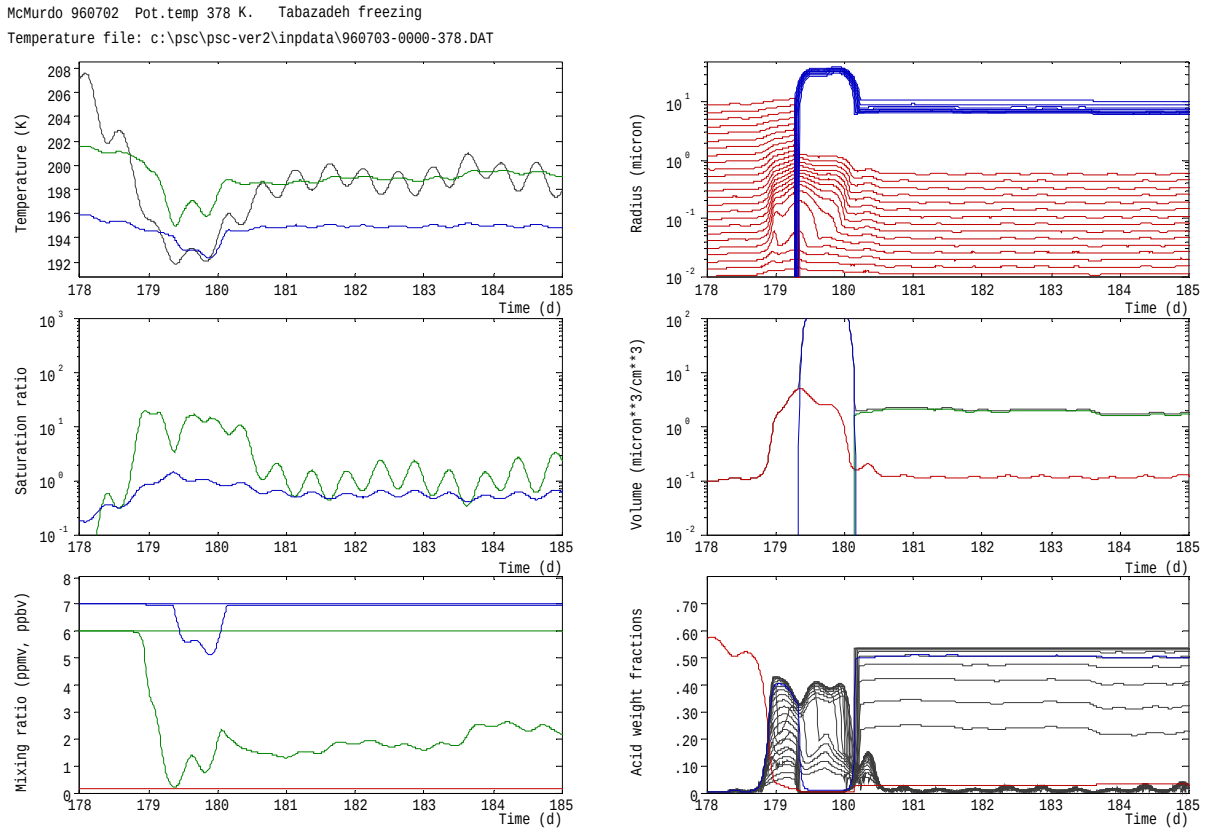

Figure 4

Another interesting example of observation/simulation (4 July 1996, case # 8) is shown in Fig. 5. In this case the lidar measurements show a 2 km broad layer around 17 km with clear mixed liquid/solid particles surrounded by solid particles above and below, cf. Fig. 1, upper right panel. In this case the freezing probably took place shortly (less than one day) before the observations which are obtained at very low temperatures. Again, in order to freeze only a fraction of the liquid particles the water vapor concentration must be adjusted so that the temperatures are just slightly below the threshold for freezing. If the H_2O concentrations were slightly higher, all particles would freeze into a fully developed type 2 PSC in contrast to observations, and for lower water concentrations no freezing would take place. Since the solid particles are observed at very low temperatures, presumable below the ice frost point, without significant growth into a fully developed NAT or ice cloud this observation might indicate a situation where freezing of STS turns these particles into a metastable dilute solid solution as a transition state to more stable type 1a NAT particles.

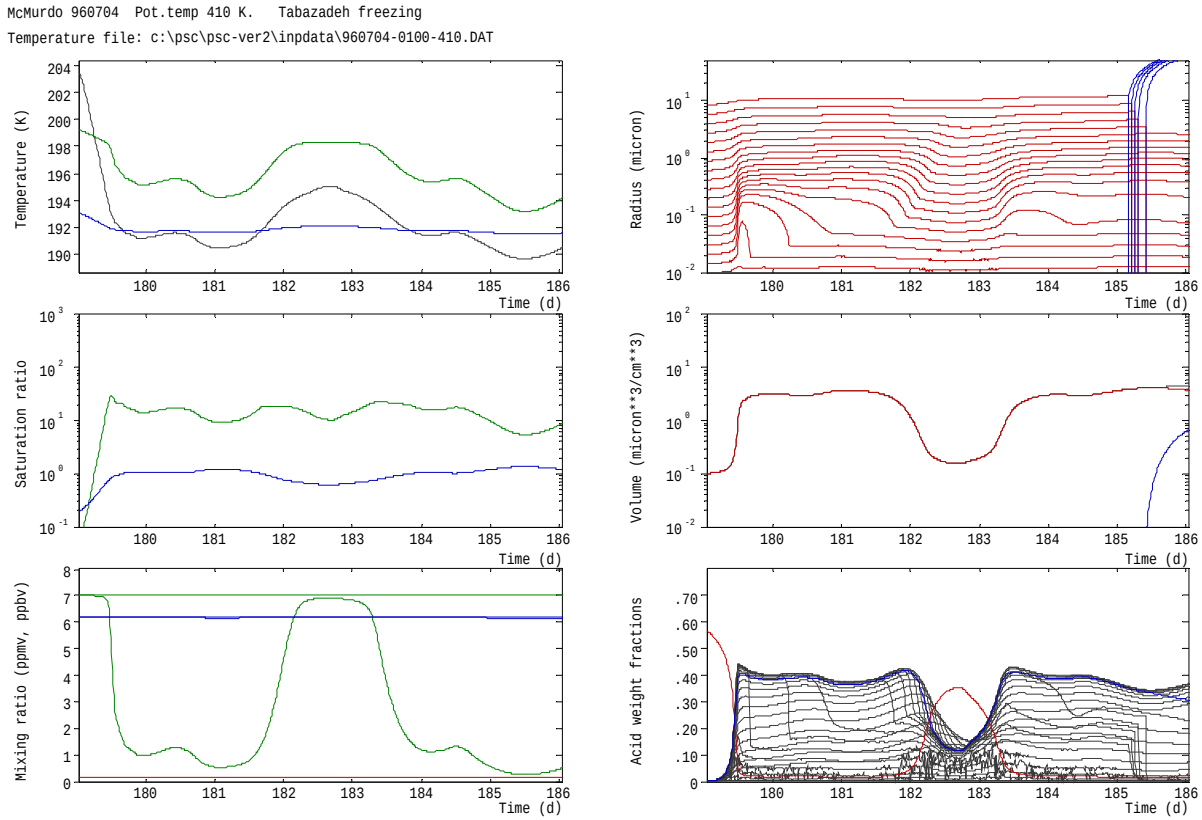

Figure 5

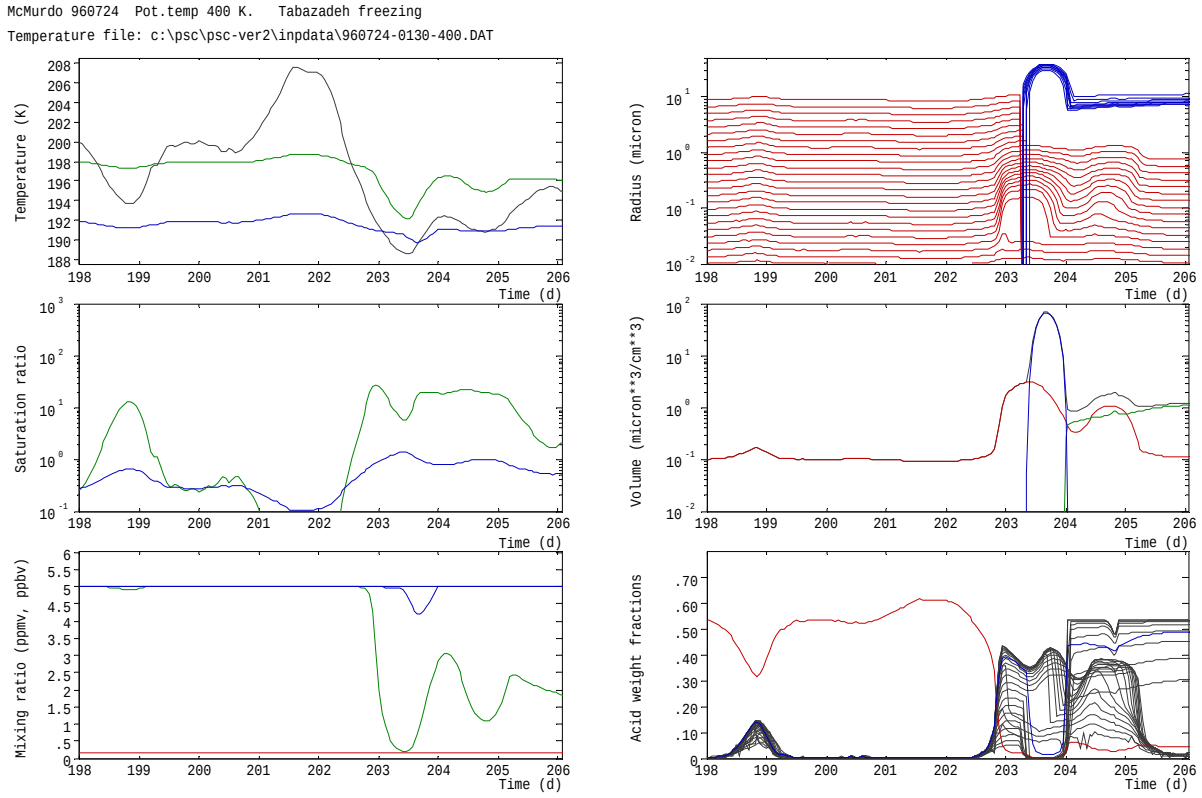

Figure 6

Fig. 6 shows a simulation of case #13 (24 July 1996) where the lidar measurements (Fig. 1, middle left panel) indicate mostly solid particles in a broad layer between 12 and 18 km and liquid particles above. The simulation shows that freezing probable took place not more than 2.5 days before observation. A fully developed NAT cloud with only a small amount of liquid volume left behind is seen at the end of the simulation in good agreement with the observations. It should be noticed that at the app. 4 K lower temperatures around day 204.75 the liquid particle volumes increase above the background and thereby also increase the liquid backscatter. This shows the potential for observing small amounts of liquid particles in a fully developed NAT cloud if the measurements are obtained at sufficiently low temperatures.

Finally, a sequence of observations at nearly the same altitude during a relatively short period in June 1997 will be discussed (cases 15, 19, and 21) with simulation results shown in Figures 7, 8, and 9. The observations on 20 June show a 2-3 km thick layer around 17 km altitude with dominantly liquid particles (Fig. 1, middle right panel). The observations on the following days (22 and 24 June) show a gradual change into dominance of solid particles at this altitude (Fig. 1, lower panels). This feature is also well represented in the simulations using the same HNO_3 and H_2O mixing ratios in the three cases (Fig. 7, 8, and 9). What is more interesting is that the temperature development around the time of freezing is nearly the same in all three cases, but the subsequent temperature development thereafter shows a gradual change. In the 20 June case the temperatures rise close to or perhaps above T_{NAT} (depending on the assumed HNO_3 mixing ratio) where the temperature in the other two cases tend to stabilize between T_{NAT} and T_{ice}. The reason that only a small fraction of the particles freeze in the 20 June simulation could be a coincidence since the temperature just barely goes below the threshold for freezing and this may not reflect the real processes. Instead, a large fraction of the particles could have frozen at the minimum temperature in all three cases. However, in the 20 June case, with dominantly liquid particles, the temperatures could have raised above T_{NAT}, evaporating the NAT and leaving behind a SAT particle. In the subsequent cooling SAT may be unstable against melting and turn into STS as expected from thermodynamical models (Koop and Carslaw, 1996). This scenario is gradually less probably for the situation in the following days and a larger fraction of the solid particles may remain as observed. The situation on 20 June is also interesting in the sense that the NAT saturation ratio raises above 15. According to laboratory measurements (Iraci et al., 1998), this condition is required to initiate the SAT dissolution into STS, but presumably followed by a gradual nucleation of NAT out of the STS solution, again forming type 1a PSC particles.

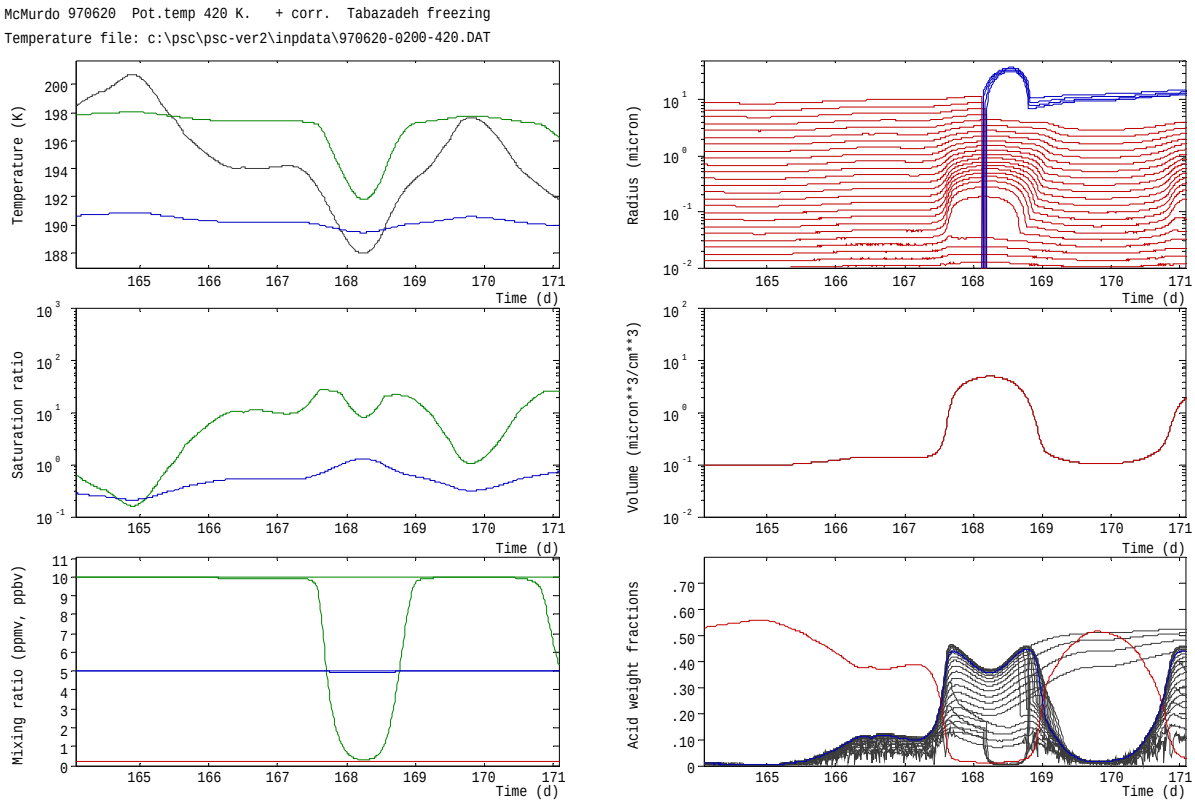

Figure 7

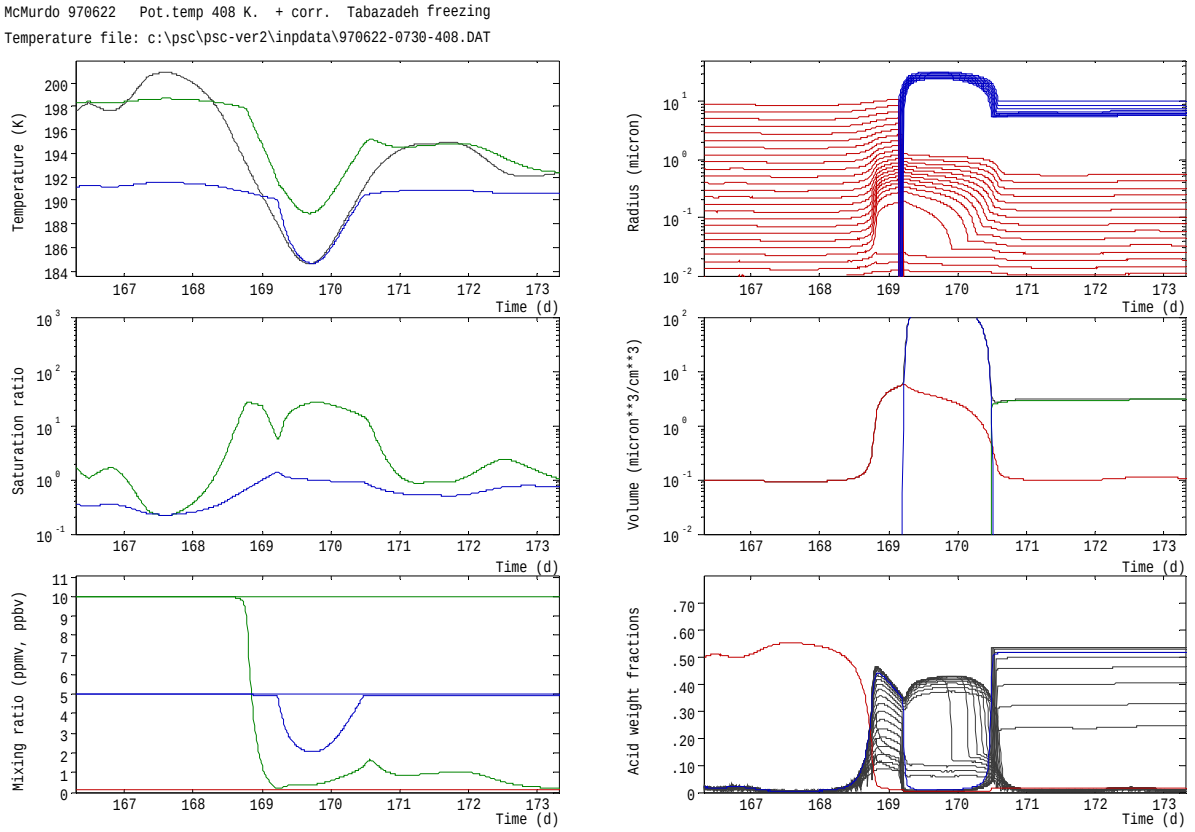

Figure 8

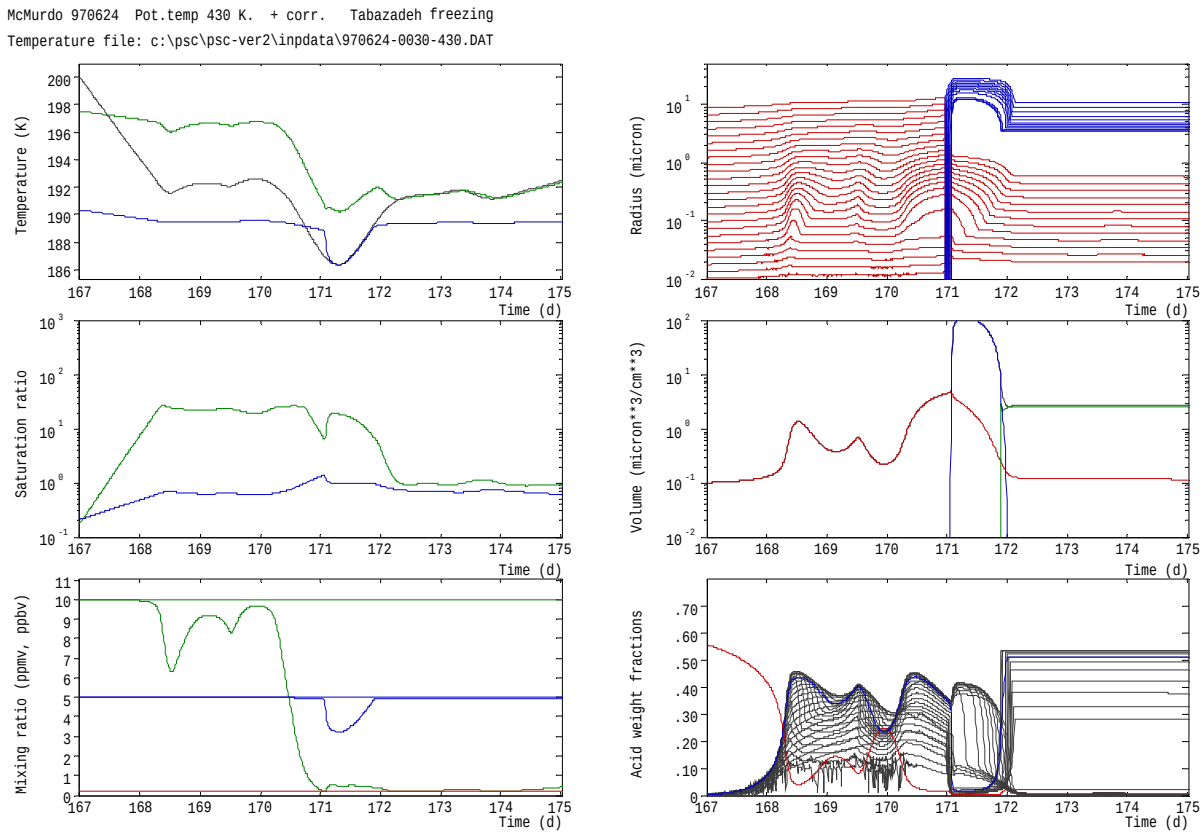

Figure 9

Summary.

Work has been initiated to identify cases among lidar observations from the Antarctic McMurdo station, showing PSCs in the state of liquid/solid phase transformations. Microphysical simulations of these situations will add substantial knowledge about the unknown but important details of freezing and melting upon cooling among PSC particles. This work is intended to be continued during the POSTCODE project. In particular, focus in the subsequent work should be directed into cases showing:

- observations with liquid/solid particle mixtures at very low temperatures and clear signatures in the trajectories of recent freezing (less than 1-2 days before observations), possibly generating solid PSC particles in a metastable state as possible indicated in case no. 8, Fig. 5.
- observations where the trajectories have indicated that freezing presumably have taken place within one week before observation, followed by temperature increases above T_{NAT}, and subsequent cooling as possibly indicated in case 15, Fig.7. These cases could be used to study the important processes of phase transformation among SAT particles, possibly leading to STS particles upon cooling or nucleation of NAT type 1a PSC particles.

A more substantial set of cases of these types will be of high value for improvements of the microphysical modeling of PSCs.

References.

Iraci, L.T., T.J. Fortin, and M.A. Tolbert, Dissolution of sulfuric acid tetrahydrate at low temperatures and subsequent growth of nitric acid trihydrate, J. Geophys. Res. 103, 8491-8498, 1998.

Koop, T. and K. S. Carslaw, Melting of H2SO4 4H2O particles upon cooling: Implications for polar stratospheric clouds, Science 272, 1638-1641, 1996.

Larsen, N., Polar stratospheric clouds: A microphysical simulation model, Scientific report 91-2, Danish Meteorological Insitute, Copenhagen, 1991.

Larsen, N. Stratospheric aerosols, Backscatter measurements from Thule, European Arctic Stratospheric Ozone Experiment, Scientific report 92-1, Danish Meteorological Institute, Copenhagen, 1992

Larsen, N., B.M. Knudsen, J.M. Rosen, N.T. Kjome, R. Neuber, and E. Kyrö: Temperature histories in liquid and solid polar stratospheric cloud formation, Journal of Geophysical Research , 102, 23505-23517, 1997.

Larsen, N. and B. Knudsen, Microphysical simulations of freezing of polar stratospheric clouds, in N. R.P. Harris, I. Kilbane-Dawe, and G.T. Amanatidis: Polar stratospheric ozone 1997, Proceedings of the fourth European symposium, 22 to 26 September 1997, Schliersee, Germany, Air polution research report 66, CEC, p. 143-146, 1998.

Luo, B., U. Krieger, and T. Peter, Densities and refractive indices of $H_2SO_4/HNO_3/H_2O$ solutions to stratospheric temperatures, Geophys. Res. Lett. 23, 3707-3710, 1996.

Tabazadeh et al., Formation and implications of ice particle nucleation in the stratosphere, Geophys. Resl. Lett. 24, 2007, 1997.

DANISH METEOROLOGICAL INSTITUTE

Scientific Reports

Scientific reports from the Danish Meteorological Institute cover a variety of geophysical fields, i.e. meteorology (including climatology), oceanography, subjects on air and sea pollution, geomagnetism, solar-terrestrial physics, and physics of the middle and upper atmosphere.

Reports in the series within the last five years:

No. 94-1
Bjørn M. Knudsen: Dynamical processes in the ozone layer.

No. 94-2
J. K. Olesen and K. E. Jacobsen: On the atmospheric jet stream with clear air turbulences (CAT) and the possible relationship to other phenomena including HF radar echoes, electric fields and radio noise.

No. 94-3
Ole Bøssing Christensen and Bent Hansen Sass: A description of the DMI evaporation forecast project.

No. 94-4
I.S. Mikkelsen, B. Knudsen, E. Kyrö and M. Rummukainen: Tropospheric ozone over Finland and Greenland, 1988-94.

No. 94-5
Jens Hesselbjerg Christensen, Eigil Kaas, Leif Laursen: The contribution of the Danish Meteorological Institute (DMI) to the EPOCH project "The climate of the 21st century" No. EPOC-003-C (MB).

No. 95-1
Peter Stauning and T.J. Rosenberg: High-Latitude, Day-time Absorption Spike Events
1. Morphology and Occurrence Statistics.
Not Published.

No. 95-2
Niels Larsen: Modelling of changes in stratospheric ozone and other trace gases due to the emission changes : CEC Environment Program Contract No. EV5V-CT92-0079. Contribution to the final report.

No. 95-3
Niels Larsen, Bjørn Knudsen, Paul Eriksen, Ib Steen Mikkelsen, Signe Bech Andersen and Torben Stockflet Jørgensen: Investigations of ozone, aerosols, and clouds in the arctic stratosphere : CEC Environment Program Contract No. EV5V-CT92-0074. Contribution to the final report.

No. 95-4
Per Høeg and Stig Syndergaard: Study of the derivation of atmospheric properties using radio-occultation technique.

No. 95-5
Xiao-Ding Yu, **Xiang-Yu Huang** and **Leif Laursen** and Erik Rasmussen: Application of the HIRLAM system in China: Heavy rain forecast experiments in Yangtze River Region.

No. 95-6
Bent Hansen Sass: A numerical forecasting system for the prediction of slippery roads.

No. 95-7
Per Høeg: Proceeding of URSI International Conference, Working Group AFG1 Copenhagen, June 1995. Atmospheric Research and Applications Using Observations Based on the GPS/GLONASS System.

No. 95-8
Julie D. Pietrzak: A Comparison of Advection Schemes for Ocean Modelling.

No. 96-1
Poul Frich (co-ordinator), H. Alexandersson, J. Ashcroft, B. Dahlström, G.R. Demarée, A. Drebs, A.F.V. van Engelen, E.J. Førland, I. Hanssen-Bauer, R. Heino, T. Jónsson, K. Jonasson, L. Keegan, P.Ø. Nordli, **T. Schmith**, **P. Steffensen**, H. Tuomenvirta, O.E. Tveito: North Atlantic Climatological Dataset (NACD Version 1) - Final Report.

No. 96-2
Georg Kjærgaard Andreasen: Daily Response of High-latitude Current Systems to Solar Wind Variations: Application of Robust Multiple Regression. Methods on Godhavn magnetometer Data.

No. 96-3

Jacob Woge Nielsen, Karsten Bolding Kristensen, Lonny Hansen: Extreme sea level highs: A statistical tide gauge data study.

No. 96-4
Jens Hesselbjerg Christensen, Ole Bøssing Christensen, Philippe Lopez, Erik van Meijgaard, Michael Botzet: The HIRLAM4 Regional Atmospheric Climate Model.

No. 96-5
Xiang-Yu Huang: Horizontal Diffusion and Filtering in a Mesoscale Numerical Weather Prediction Model.

No. 96-6
Henrik Svensmark and Eigil Friis-Christensen:
Variation of Cosmic Ray Flux and Global Cloud Coverage - A Missing Link in Solar-Climate Relationships.

No. 96-7
Jens Havskov Sørensen and Christian Ødum Jensen: A Computer System for the Management of Epidemiological Data and Prediction of Risk and Economic Consequences During Outbreaks of Foot-and-Mouth Disease. CEC AIR Programme. Contract No. AIR3 - CT92-0652.

No. 96-8
Jens Havskov Sørensen: Quasi-Automatic of Input for LINCOM and RIMPUFF, and Output Conversion. CEC AIR Programme. Contract No. AIR3 - CT92-0652.

No. 96-9
Rashpal S. Gill and Hans H. Valeur:
Evaluation of the radarsat imagery for the operational mapping of sea ice around Greenland.

No. 96-10
Jens Hesselbjerg Christensen, Bennert Machenhauer, Richard G. Jones, Christoph Schär, Paolo Michele Ruti, Manuel Castro and Guido Visconti:
Validation of present-day regional climate simulations over Europe: LAM simulations with observed boundary conditions.

No. 96-11
Niels Larsen, Bjørn Knudsen, Paul Eriksen, Ib Steen Mikkelsen, Signe Bech Andersen and Torben Stockflet Jørgensen: European Stratospheric Monitoring Stations in the Artic: An European contribution to the Network for Detection of Stratospheric Change (NDSC): CEC Environment Programme Contract EV5V-CT93-0333: DMI contribution to the final report.

No. 96-12
Niels Larsen: Effects of heterogeneous chemistry on the composition of the stratosphere: CEC Environment Programme Contract EV5V-CT93-0349: DMI contribution to the final report.

No. 97-1
E. Friis Christensen og C. Skøtt: Contributions from the International Science Team. The Ørsted Mission - A Pre-Launch Compendium.

No. 97-2
Alix Rasmussen, Sissi Kiilsholm, Jens Havskov Sørensen, Ib Steen Mikkelsen: Analysis of Tropospheric Ozone Measurements in Greenland: Contract No. EV5V-CT93-0318 (DG 12 DTEE): DMI's contribution to CEC Final Report Arctic Trophospheric Ozone Chemistry ARCTOC.

No. 97-3
Peter Thejll: A Search for Effects of External Events on Terrestrial Atmospheric Pressure: Cosmic Rays

No. 97-4
Peter Thejll: A Search for Effects of External Events on Terrestrial Atmospheric Pressure: Sector Boundary Crossings

No. 97-5
Knud Lassen: Twentieth Century Retreat of Sea-Ice in the Greenland Sea

No. 98-1
Niels Woetman Nielsen, Bjarne Amstrup, Jess U. Jørgensen:
HIRLAM 2.5 parallel tests at DMI:
Sensitivity to type of schemes for turbulence, moist processes and advection

No. 98-2
Per Høeg, Georg Bergeton Larsen, Hans-Henrik Benzon, Stig Syndergaard, Mette Dahl Mortensen:
The GPSOS project
Algorithm Functional Design and Analysis of ionosphere, Stratosphere and Troposphere Observations

No. 98-3
Dahl Mortensen, Mette; Per Høeg:
Satellite Atmosphere Profiling Retrieval in a Nonlinear Troposphere
Previously entitled: Limitations Induced by Multipath

No. 98-4

Dahl Mortensen, Mette Per Høeg:
Resolution Properties in Atmospheric Profiling with GPS

No. 98-5
Gill, R. S. and M. K. Rosengren
Evaluation of the Radarsat Imagery for the Operational Mapping of Sea Ice around Greenland in 1997.

No. 98-6
Gill, R. S., Valeur, H. H., Nielsen, P. and Hansen, K. Q.: Using ERS SAR images in the operational mapping of sea ice in the Greenland waters: final report for ESA-ESRIN's: pilot projekt no. PP2.PP2.DK2 and 2nd Announcement of opportunity for the exploitation of ERS data projekt No. AO2..DK 102.

No. 98-7
Høeg, Per et al.: GPS Atmosphere Profiling Methods and Error Assessments.

No. 98-8
Svensmark, H., N. Woetmann Nielsen and A.M. Sempreviva: Large Scale Soft and Hard Turbulent States of the Atmosphere.

No. 98-9
Lopez, Philippe, Eigil Kaas and Annette Guldberg: The Full Particle-In-Cell advection scheme in spherical geometry**.**

No. 98-10
Svensmark, H.: Influence of Cosmic Rays on Earth's Climate.

No. 98-11
Thejll, Peter and Henrik Svensmark: Notes on the method of normalized multivariate regression.

No. 98-12
Lassen. K: Extent of sea ice in the Greenland Sea 1977-1997: an extension of DMI Scientific Report 97-5

No. 98-13
Larsen, Niels; Adriani, Alberto and Donfrancesco, Guido Di: Microphysical analysis oof plar stratospheric clouds observed by Lidar at McMurco, Antarctica

No.98-14
Dahl Mortensen, Mette: The Back-Propagation Method for Inversion of Radio Occultation Data.